crystals

MDPI

Article

Cocrystals of Isoniazid with Polyphenols: Mechanochemical Synthesis and Molecular Structure

Juan Saulo González-González [1,*], Ana María Monserrat Martínez-Santiago [1], Francisco Javier Martínez-Martínez [2], María José Emparán-Legaspi [2], Armando Pineda-Contreras [2], Marcos Flores-Alamo [3] and Héctor García-Ortega [3,*]

1 Instituto de Farmacobiología, Universidad de la Cañada, Carretera Teotitlán-San Antonio Nanahuatipán km 1.7 s/n., Paraje Titlacuatitla, Teotitlán de Flores Magón, 68540 Oaxaca, Mexico; santi_mon12@hotmail.com

2 Facultad de Ciencias Químicas, Universidad de Colima, km 9 Carretera Colima-Coquimatlán, Coquimatlán, 28400 Colima, Mexico; fjmartin@ucol.mx (F.J.M.-M.); mj_emparan@hotmail.com (M.J.E.-L.); armandop@ucol.mx (A.P.-C.)

3 Facultad de Química, Universidad Nacional Autónoma de México, 04510 Ciudad de México, Mexico; mfa@unam.mx

* Correspondence: juan_saulo@unca.edu.mx (J.S.G.-G.); hector.garcia@unam.mx (H.G.-O.)

Received: 28 May 2020; Accepted: 29 June 2020; Published: 2 July 2020

Abstract: Isoniazid is used as anti-tuberculosis drug which possesses functional groups capable of forming hydrogen bonds. A series of cocrystals of isoniazid (INH) with polyphenolic coformers such as catechol (CAT), orcinol (ORC), 2-methylresorcinol (MER), pyrogallol (PYR), and phloroglucinol (PLG) were prepared by solvent-assisted grinding. Powder cocrystals were characterized by infrared (IR) spectroscopy and X-ray powder diffraction. The crystal structure of the cocrystals revealed the unexpected hydration of the INH-MER cocrystal and the preference of the (phenol) O–H···N (pyridine) and (terminal) N-H···O (phenol) heterosynthons in the stabilization of the structures. The supramolecular architecture of the cocrystals is affected by the conformation and the substitution pattern of the hydroxyl groups of the polyphenols.

Keywords: isoniazid; cocrystal; polyphenols; hydrogen bond; mechanochemistry

1. Introduction

The modification of solid forms of pharmaceutical active ingredients has led to the formation of polymorphs, salts, solvates, and cocrystals to improve physico-chemical properties, such as solubility, dissolution rate, melting point, and thermal stability [1]. Pharmaceutical cocrystals are crystalline solids formed by a pharmaceutical active ingredient and a cocrystal coformer, which remain together by noncovalent interactions—principally hydrogen bonds [2]. Crystal engineering concepts are employed in the design of pharmaceutical cocrystals considering the use of supramolecular synthons between the functional groups of the compounds involved in the formation of the cocrystal, leading to directional and geometrical well-defined hydrogen bond patterns [3].

Solvent-assisted grinding and solvent evaporation are two commonly used methods for cocrystal synthesis [4]. Solvent-assisted grinding is a fast method for obtaining powder cocrystals. The advantage of this method is that it does not depend on the solubility of the starting materials. However, not all grinding experiments lead to the formation of powder cocrystals. On the other hand, the solvent evaporation method is used to obtain single crystals of cocrystals and cocrystals that cannot be prepared by grinding experiments. The disadvantages of this method are the dependence of the solubility of the starting materials and the waiting time for the evaporation of the solvent.

Isoniazid is used as an anti-tuberculosis drug [5]; however, its irrational use has led to the development of bacterial resistance [6]. Its chemical structure possesses pyridine and hydrazide

functional groups capable of forming hydrogen bonds, leading to the formation of supramolecular homosynthons (hydrazide-hydrazide) and heterosynthons (acid-pyridine, hydroxyl-pyridine, amide-amide, hydroxyl-amide). Cocrystals of isoniazid have been prepared using nicotinamide, dicarboxylic acids, and hydroxybenzoic acids as coformers [7–10].

On the other hand, polyphenols (dihydroxy and trihydroxy benzenes) have been used as antibacterial agents [11,12] and as cocrystal coformers due to their ability to form O-H···O and O-H···N hydrogen bonds. Some examples of pharmaceutical cocrystals involving polyphenols as coformers are resorcinol-theophylline; phloroglucinol-lidocaine; catechol, resorcinol, and pyrogallol with tenoxicam; resorcinol and pyrogallol with curcumin; and resorcinol and orcinol with artemisinin [13–17].

Here, we report the mechanochemical synthesis, characterization, and crystal structure of cocrystals of isoniazid (INH) with the polyphenolic coformers catechol (CAT), orcinol (ORC), 2-methylresorcinol (MER), pyrogallol (PYR), and phloroglucinol (PLG) as potential anti-tuberculosis agents (Figure 1).

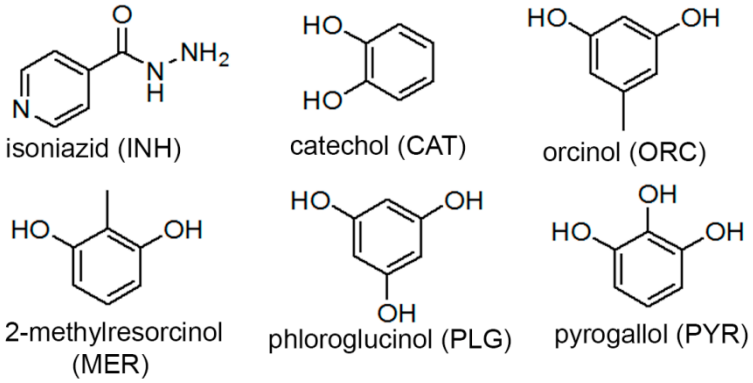

Figure 1. Compounds used in the cocrystallization study.

2. Materials and Methods

2.1. Liquid-Assisted Grinding and Crystallization

Isoniazid (99.0%), orcinol (97%), 2-methylresorcinol (98%), catechol (99.0%), phloroglucinol (99.0%), and pyrogallol (98.0%) were purchased from Aldrich (St. Louis, MO, USA). Ethanol (ACS grade) and dichloromethane (ACS grade) were purchased from Quimica Meyer (Mexico City, Mexico). All the reagents and solvents were used as received.

Mixtures in a 1:1 ratio of INH (300 mg, 2.1 mmol) and the polyphenolic coformer (2.1 mmol, ORC = 273 mg; MER = 273 mg; CAT = 242 mg; PLG = 277 mg; PYR = 277 mg) were ground in a porcelain mortar with a pestle. Before the start of the grinding, 0.5 mL of dichloromethane was added. After 3 min of grinding, dichloromethane evaporated, and the powder was collected. The cycle of adding dichloromethane (0.5 mL) and grinding for 3 min was repeated an additional three times until 12 min of grinding was completed. After that, a polycrystalline powder was obtained. The grinding process was performed in a laboratory hood to eliminate the residual dichloromethane.

Single crystals of INH-ORC, INH-MER–H_2O, INH-CAT, INH-PLG, and INH-PYR suitable for X-ray diffraction were obtained by dissolving 50 mg of the respective polycrystalline ground powder in ethanol and left to evaporate at room temperature.

2.2. Infrared Spectroscopy

Infrared spectra of the solid powders of INH, ORC, MER, CAT, PLG, and PYR, the polycrystalline ground powders, and the single crystals were obtained in a Bruker Tensor 27 spectrophotometer (Bruker, Ettlingen, Germany) equipped with an attenuated total reflection (ATR) system accessory (16 scans, spectral range 600–4000 cm^{-1}, resolution 4 cm^{-1}).

2.3. X-ray Diffraction

X-ray powder diffraction patterns of INH, ORC, MER, CAT, PLG, PYR, and the polycrystalline ground powders were acquired in a PANalytical X'Pert PRO diffractometer (Almelo, The Netherlands) with Cu Kα_1 radiation (λ = 1.5405 Å, 45 kV, 40 mA) from 2.02° to 49.93° in 2θ.

The crystal structure of the cocrystals was analyzed in an Oxford Diffraction Gemini "A" diffractometer (Oxford Diffraction, Oxfordshire, UK) with a CCD area detector ($\lambda_{MoK\alpha}$ = 0.71073 Å, monochromator). Crystal data, data collection, and structure refinement details are summarized in Table 1. Unit cell parameters were determined with a set of three runs of 15 frames (1° in ω). The double-pass method of scanning was used to exclude any noise. The collected frames were integrated using an orientation matrix determined from the narrow frame scans. CrysAlisPro and CrysAlis RED software packages [18] were used for data collection and integration. Analysis of the integrated data did not reveal any decay. Final cell parameters were determined by a global refinement of 1674, 1815, 1842, 2721, and 1620 reflections (3.519° < θ < 29.50°) for compounds INH-ORC, INH-MER, INH-CAT, INH-PLG, and INH-PYR respectively. Collected data were corrected for absorption effects by using an analytical numeric absorption correction [19] using a multifaceted crystal model based on expressions upon the Laue symmetry using equivalent reflections. Structure solution and refinement were carried with the programs SHELXS-2014 [20] and SHELXL-2014 [21] respectively. WinGX v2014.1, Ortep [22], and Mercury [23] software were used to prepare material for publication. Full-matrix least-squares refinement was carried out by minimizing $(Fo^2 - Fc^2)^2$. All nonhydrogen atoms were refined anisotropically. The H atoms of the hydroxy and amine groups were located in a difference map and refined isotropically with Uiso(H) = 1.5 for H–O and Uiso(H) = 1.2 for H–N. Hydrogen atoms attached to carbon atoms were placed in geometrically idealized positions and refined as riding on their parent atoms, with C–H = 0.95–0.98 Å with Uiso(H) = 1.2 Ueq(C) for aromatic groups and Uiso(H) = 1.5 Ueq(C) for methyl groups. Crystallographic data have been deposited at the Cambridge Crystallographic Data Center as supplementary material number CCDC 1989808–1989812.

Table 1. Crystallographic data and refinement for the isoniazid (INH) cocrystals.

Cocrystal	INH-ORC	INH-MER-H_2O	INH-CAT	INH-PLG	INH-PYR
Molecular formula	$C_6H_7N_3O{\cdot}C_7H_8O_2$	$C_6H_7N_3O{\cdot}C_7H_8O_2{\cdot}H_2O$	$C_6H_7N_3O{\cdot}C_6H_6O_2$	$C_6H_7N_3O{\cdot}C_6H_6O_3$	$C_6H_7N_3O{\cdot}C_6H_6O_3$
Mr Formula weight (g·mol^{-1})	261.28	279.29	302.31	400.40	263.25
Crystal system	Monoclinic	Monoclinic	Monoclinic	Monoclinic	Triclinic
Space group	$P2_1/n$	$P2_1/c$	$P2/c$	$P2_1/c$	P-1
a, b, c (Å)	7.3607(9), 13.2387(14), 12.9532(17)	10.2646(8), 6.8865(5), 19.0382(13)	17.5391(13), 7.0947(5), 12.1518(9)	7.1867(5), 9.1733(7), 27.751(2)	7.7020(6), 8.2347(11), 10.6669(15)
α, β, γ (°)	90, 92.118(11), 90	90, 94.671(8), 90	90, 108.616(8), 90	90, 92.721(7),90	107.521(12), 107.527(10), 97.396(9)
V (Å^3)	1261.4(3)	1341.29(17)	1432.99(19)	1827.4(2)	597.02(13)
Z	4	4	4	4	2
μ (mm^{-1})	0.100	0.104	0.104	0.109	0.112
T (K)	130(2)	130(2)	130(2)	130(2)	130(2)
ρ_{calcd} (g·cm^{-3})	1.376	1.383	1.401	1.455	1.464
Crystal size (mm)	0.470 × 0.320 × 0.210	0.550 × 0.420 × 0.320	0.480 × 0.380 × 0.260	0.460 × 0.370 × 0.290	0.460 × 0.370 × 0.290
F(000)	552	592	636	840	276
θ range (°)	3.457–29.354	3.566–29.548	3.538–29.358	3.604–29.502	3.884–29.424
Reflections collected	5891	5919	6477	9139	4443
Independent reflections	2934	3143	3368	4305	2768
Data/restraints/parameters	2934/5/188	3143/7/204	3368/6/217	4305/9/289	2768/6/190
Goof	1.004	1.022	1.015	0.962	1.039
R (int)	0.0269	0.0235	0.0250	0.0323	0.0235
Final R indices [I > 2σ(I)], R1/wR2	0.0492/0.1184	0.0452/0.0966	0.0472/0.1013	0.0548/0.1327	0.0455/0.1036
Largest diff. peak/hole (e·Å^{-3})	0.354/0.312	0.266/−0.288	0.407/−0.283	0.292/−0.393	0.310/−0.332

3. Results and Discussion

3.1. IR Spectroscopy

IR spectroscopy is a tool used to identify the formation of new solid phases by the shift of the bands of the functional groups of the cocrystal with respect to the starting products. Characteristic bands of the functional groups of the compounds were assigned according with previous reports [14,24–26]. The IR spectra of the ground powders were different with respect to the starting materials (Figures

S1–S5 Supplementary Materials), suggesting the cocrystal formation. The IR spectra of the ground powders and the single crystals were similar (Figure 2), indicating structural homogeneity between the polycrystalline ground powder and the single crystal.

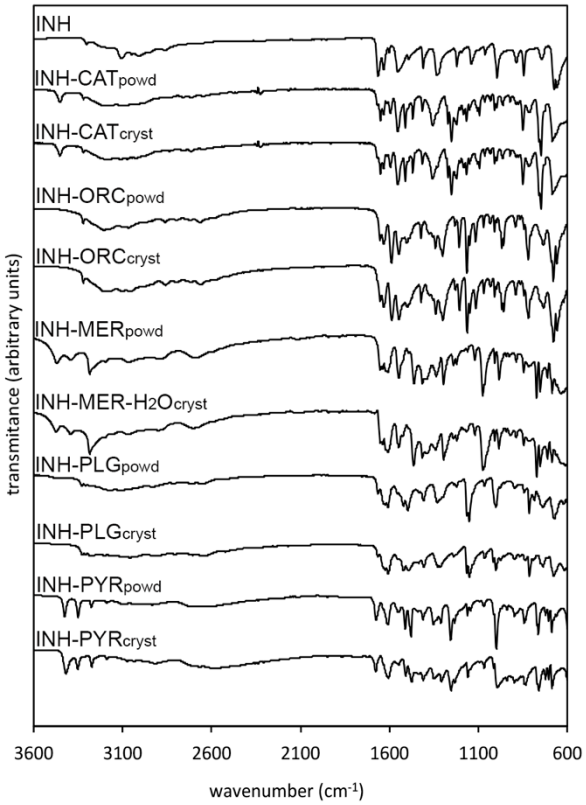

Figure 2. IR spectra of the polycrystalline ground powders and the single crystals.

The amine N-H, carbonyl C=O, hydroxyl O–H, and pyridine C=N stretching frequencies of INH were observed to have shifted in the IR spectra of the polycrystalline ground powders and the single crystals as a consequence of the formation of intermolecular hydrogen bonds, due to the rearrangement of the crystalline structure (Table S1 Supplementary Materials). The IR spectra of INH showed the N-H stretching band at 3303 cm^{-1}; meanwhile the IR spectra of the polycrystalline ground powders and the single crystals appeared shifted to higher frequencies (from 3322 cm^{-1} to 3397 cm^{-1}). The C=O stretching band appeared at 1662 cm^{-1} in "free INH" while the polycrystalline ground powders and the single crystals appeared shifted from 1651 cm^{-1} to 1676 cm^{-1}. The pyridine C=N stretching band in INH also was shifted from 1553 cm^{-1} in "free" INH to the 1543 cm^{-1}–1556 cm^{-1} range in the new solid form, suggesting the formation of the O–H···N hydrogen bond. The hydroxyl O–H stretching frequencies of the polyphenols were also shifted due to the formation of the O–H···N and O-H···O=C intermolecular hydrogen bonds ($\Delta\nu$O–H = 6–191 cm^{-1}).

3.2. Powder X-ray Diffraction

PXRD patterns of the polycrystalline ground mixtures were different from the starting materials (Figures S6–S10 Supplementary Materials), indicating the formation of the cocrystal. PXRD patterns of the ground products were similar to the theoretical PXRD patterns calculated with Mercury [23], indicating an adequate homogeneity between the ground mixture and the single crystal (Figure 3).

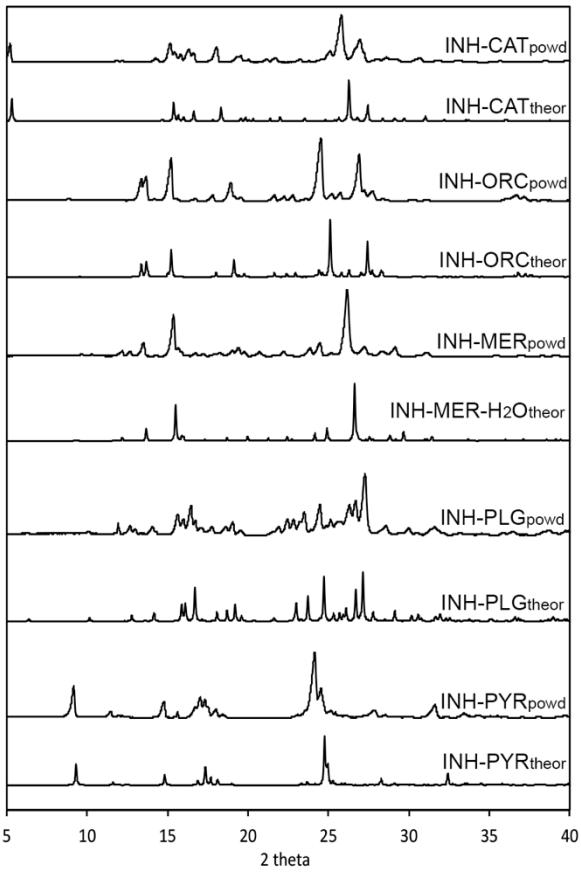

Figure 3. Powder X-ray diffraction patterns of the polycrystalline powders (collected at 25.0 °C) and the theoretical calculated with Mercury (collected at −143.15 °C).

3.3. Crystal Structure

The geometric parameters associated with intermolecular non-covalent interactions D–H···A are summarized in Table 2. Classic hydrogen bonding interactions and π-stacking are in agreement with accepted criteria [27,28]. Hydrogen bond patterns are described according to graph set notation [29]. Possible conformations of polyphenols [30–33] and supramolecular synthons are shown in Figures 4 and 5, respectively.

Table 2. Hydrogen bond geometry (Å, °) for the INH cocrystals.

Cocrystal	Interaction	D-H	H···A	D···A	D-H···A	Symmetry Code
INH-ORC	N1-H1···N2	0.916(16)	2.127(17)	2.982(2)	155.0(18)	−x, −y, 1 − z
	N2-H2A···O3	0.903(17)	2.352(17)	3.104(2)	140.6(16)	$\frac{1}{2}$ − x, −1/2 + y, $\frac{1}{2}$ − z
	N2-H2B···O2	0.921(16)	2.165(17)	3.031(2)	156.3(16)	1 − x, −y, 1 − z
	O2-H2···O1	0.850(2)	1.900(2)	2.737(17)	166.0(2)	$\frac{1}{2}$ + x, $\frac{1}{2}$ − y, $\frac{1}{2}$ + z
	O3-H3···N3	0.870(2)	1.880(2)	2.7459(19)	170.0(19)	1 − x, 1 − y, 1 − z
INH-MER-H_2O	O3-H3···N3	0.900(18)	1.849(18)	2.7371(18)	168.8(19)	1 + x, y, z
	O2-H2···N2	0.858(15)	1.926(17)	2.7540(19)	161.7(19)	−1 + x, $\frac{1}{2}$ − y, $\frac{1}{2}$ + z
	O4-H4A···O2	0.870(2)	1.930(2)	2.7585(18)	159.0(3)	−x, −1/2 + y, $\frac{1}{2}$ − z
	O4-H4B···O1	0.860(2)	1.920(2)	2.7723(17)	174.0(2)	1 − x, 1 − y, −z
	N2-H2B···O4	0.914(19)	2.170(18)	3.0207(19)	154.4(17)	1 + x, y, z
	N1-H1···O4	0.902(14)	2.017(14)	2.8908(19)	163.0(17)	1 − x, −y, −z

Table 2. *Cont.*

Cocrystal	Interaction	D-H	H···A	D···A	D-H···A	Symmetry Code
INH-CAT	O4-H4···O3	0.840(2)	2.060(2)	2.8041(18)	147.0(2)	$1-x, y, \frac{1}{2}-z$
	O3-H3···O1	0.859(18)	1.808(18)	2.6570(16)	169.0(2)	$x, 1-y, -1/2+z$
	N2-H2B···O4	0.908(16)	2.231(18)	3.0241(19)	145.6(15)	$1-x, 1-y, 1-z$
	N1-H1···N2	0.893(16)	2.067(17)	2.896(2)	154.1(17)	$1-x, y, \frac{1}{2}-z$
	O2-H2···N3	0.879(17)	1.882(17)	2.7419(18)	165.6(19)	$x, 1-y, \frac{1}{2}+z$
	N2-H2A···O1	0.914(16)	2.231(18)	3.0637(19)	151.3(18)	$1-x, -y, 1-z$
	N2-H2B···O4	0.908(16)	2.231(18)	3.0241(19)	145.6(15)	$1-x, 1-y, 1-z$
INH-PLG	O4-H4···N6	0.859(17)	1.880(17)	2.738(2)	179.0(3)	$1-x, \frac{1}{2}+y, \frac{1}{2}-z$
	O3-H3···N3	0.868(17)	1.931(17)	2.794(2)	173.0(3)	$1-x, -1/2+y, \frac{1}{2}-z$
	O5-H5···N5	0.870(2)	1.920(2)	2.780(2)	174.0(3)	$1-x, -y, -z$
	N4-H4···O1	0.930(2)	2.000(2)	2.900(2)	165.0(2)	$1+x, -1+y, z$
	N5-H5B···O2	0.918(15)	2.150(2)	2.903(3)	139.0(2)	$1-x, -y, -z$
	N1-H1···N2	0.910(2)	2.160(2)	2.976(3)	148.4(19)	$1-x,1-y, -z$
	N2-H2A···O2	0.917(19)	2.170(2)	3.058(2)	164.0(2)	$1-x, 1-y, -z$
	N2-H2B···O5	0.923(15)	2.284(17)	3.075(3)	143.0(2)	$-x, 1-y, -z$
INH-PYR	O2-H2···O4	0.860(2)	1.980(2)	2.7160(18)	143.0(2)	$2-x, 1-y, -z$
	N1-H1···O2	0.882(17)	2.147(17)	2.913(2)	144.9(16)	
	O4-H4···N2	0.871(19)	1.844(19)	2.707(2)	170.8(19)	$1-x, 2-y, -z$
	O3-H3···N3	0.890(2)	1.860(2)	2.742(2)	175.0(2)	$1-x, 1-y, 1-z$
	N2-H2B···O1	0.900(17)	2.190(18)	2.886(2)	133.7(16)	$2-x, 1-y, -z$
	N2-H2A···O3	0.908(17)	2.245(17)	3.146(2)	172.0(2)	$1-x, 1-y, -z$

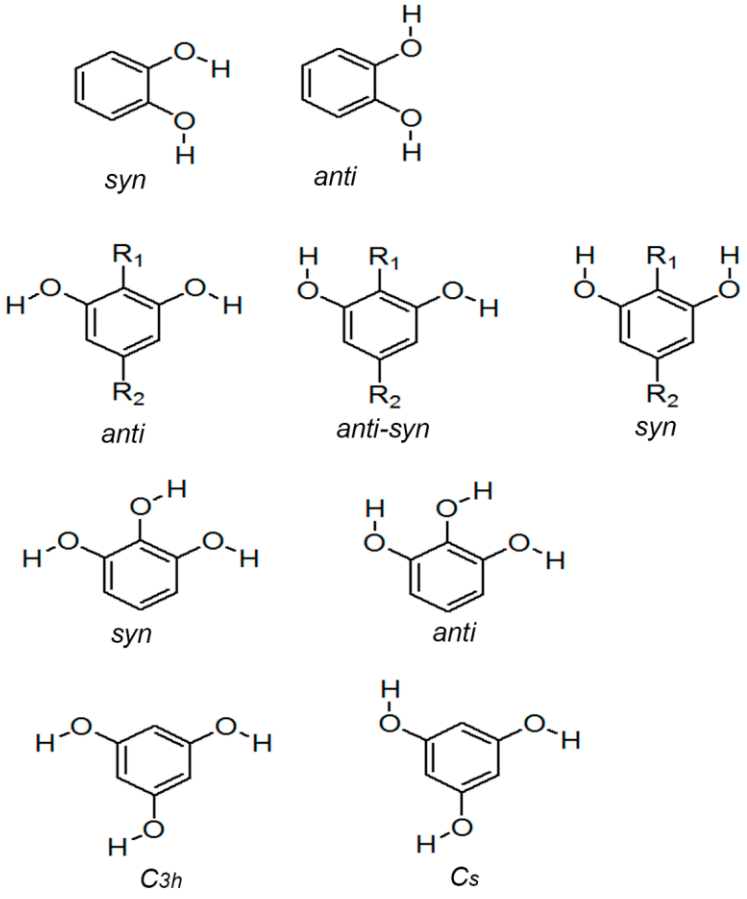

Figure 4. Possible conformations of the polyphenols used in this study.

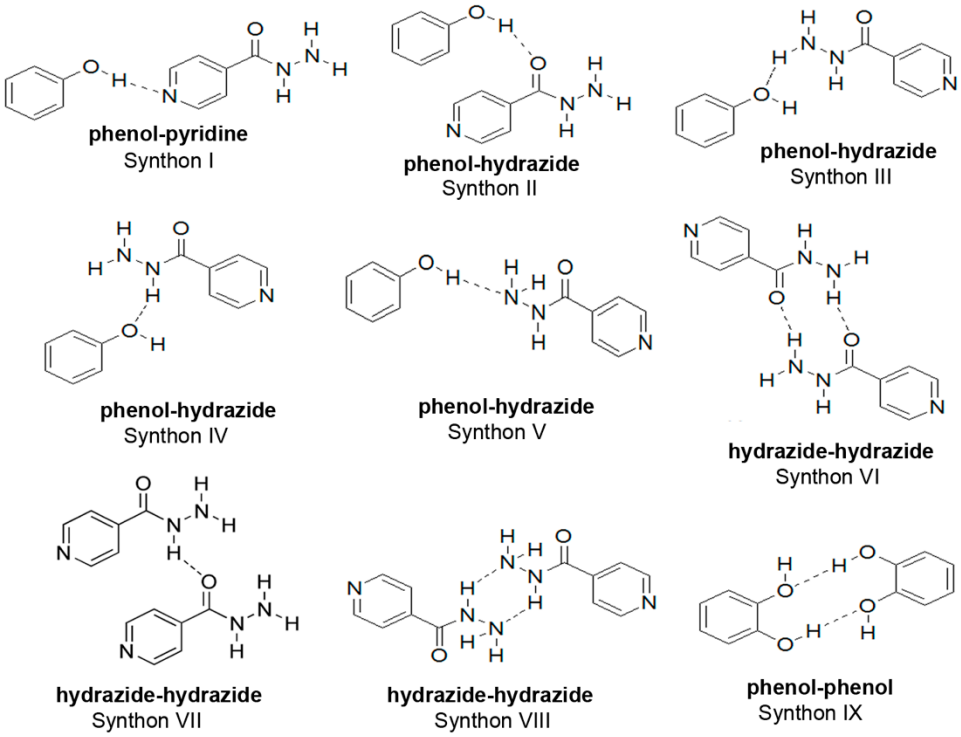

Figure 5. Supramolecular synthons found in the isoniazid-polyphenol cocrystals.

INH-ORC cocrystal. The isoniazid-orcinol cocrystal crystallizes in a $P2_1/n$ space group with one molecule of INH and one molecule of ORC in the asymmetric unit. Each molecule of ORC in the *syn* conformation is interlinked with two INH molecules by the O3–H3···N3 (synthon I) and O2–H2···O1 (synthon II) hydrogen bonds. The angle between the pyridine ring and the hydroxyl group plane is −23.0° (C4–N3–H3–O3 torsion angle). The N2–H2B···O2 hydrogen bond (synthon III) extends the supramolecular array forming a ribbon extended along the *b* axis, depicting a $R^4_4(20)$ motif. The *syn* conformation of ORC (Figure 6a) led to the formation of a finite supramolecular array in INH-ORC in contrast with the INH-RES cocrystal [8], which forms linear tapes because RES adopts a *syn-anti* conformation. The second dimensional supramolecular architecture is given by the interlinking of ribbons by the N1-H1···N2 $R^2_2(6)$ (synthon VI) hydrogen bonds along the (1 0 1) plane (Figure 6b). N2–H2A···O3 hydrogen bond (synthon III) and π-stacking ($Cg1\cdots Cg2$ = 3.624(10) Å, $Cg1$ = N3/C4/C3/C2/C6/C5; $Cg2$ = C7/C8/C9/C10/C11/C12) extend the supramolecular array in the third dimension along the *ab* plane (Figure 6c).

INH-MER–H_2O cocrystal. Unexpected hydration of the INH-MER cocrystal was found after the single-crystal X-ray diffraction study. IR spectra and PXRD patterns of the INH-MER ground with dichloromethane is similar to the IR spectra and the theoretical PXRD pattern of INH-MER–H_2O single crystal, suggesting the incorporation of water from the environment into the crystalline structure during the grinding process, obtaining the hydrated cocrystal. Polyphenols such as orcinol, phloroglucinol and pyrogallol are hygroscopic [33–35]; therefore, it is not rare to obtain hydrated cocrystals of polyphenols. Some examples are theophylline with resorcinol, orcinol and phloroglucinol [13]; nalidixic acid with phloroglucinol [36]; and lidocaine with phloroglucinol [14].

The INH-MER–H_2O cocrystal hydrate crystallizes in the monoclinic $P2_1/c$ space group with one molecule of INH, one molecule of MER adopting the *anti* conformation, and one molecule of water in the asymmetric unit. A supramolecular infinite $C^2_4(21)$ chain, similar to the INH-RES cocrystal [8], is formed when one hydroxyl group of MER is linked to an INH molecule by the O3–H3···N3 (synthon I) hydrogen bond and another hydroxyl group of MER forms the O2–H2···N2 (synthon V) hydrogen bond. Here the *anti* conformation favors the formation of an infinite chain. The angle between the pyridine ring and the hydroxyl group plane is 166.77° (C4–N3–H3A–O3 torsion angle). Water molecules

link the INH-MER chains by O4–H4A···O2, O4–H4B···O1, and N1–H1···O4 hydrogen bonds to give a two-dimensional supramolecular sheet extended along the (1 0 2) plane (Figure 7a). The whole supramolecular assembly is given by pairing sheets linked by the N2–H2B···O4 hydrogen bond and π-stacking (*Cg*1···*Cg*2 = 3.512(9) Å, *Cg*1 = N3/C4/C3/C2/C6/C5; *Cg*2 = C7/C8/C9/C10/C11/C12) (Figure 7b).

INH-CAT cocrystal. The isoniazid-catechol cocrystal crystallizes in the monoclinic *P2/c* space group, with one molecule of INH and one and a half different molecules of CAT in the asymmetric unit. A dimeric unit of CAT (synthon IX) in the *syn* conformation is formed via O4–H4···O3 $R^2_2(10)$ hydrogen bonds (CAT also form the O4–H4···O3 *S(5)* intramolecular hydrogen bond). INH molecules are linked to the catechol dimer by the N2–H2B···O4 (synthon III) and O3–H3···O1 (synthon II) hydrogen bonds to form an INH_2–CAT_2 centrosymmetric tetramer depicting a set of $R^3_3(9)$, $R^2_2(10)$, *S(5)* hydrogen bond motifs, similar to those observed in the isoniazid-caffeic acid cocrystal [8]. The first dimensional array is given by the interlinking of tetramers by the N1–H1···N2 (synthon VIII) hydrogen bonds forming a supramolecular tape running along the *c* axis (Figure 8a). Tapes are connected by the second crystallographic independent molecule of CAT, which forms two O2–H2···N3 (synthon I) hydrogen bonds extending a bidimensional supramolecular sheet along the *ac* plane (Figure 8b). The angle between the pyridine ring and the hydroxyl group plane is 19.56° (C4–N3–H2–O2 torsion angle). The interlinking of sheets by the N2–H2A···O1 (synthon VI), N2–H2B···O4 (synthon III) hydrogen bonds, and π-stacking (*Cg*1···*Cg*3 = 3.737(10) Å; *Cg*1···*Cg*3 = 3.750(10) Å; *Cg*1 = N3/C4/C3/C2/C6/C5; *Cg*3 = C7/C8/C9/C10/C11/C12) give the third dimensional supramolecular array (Figure 8c).

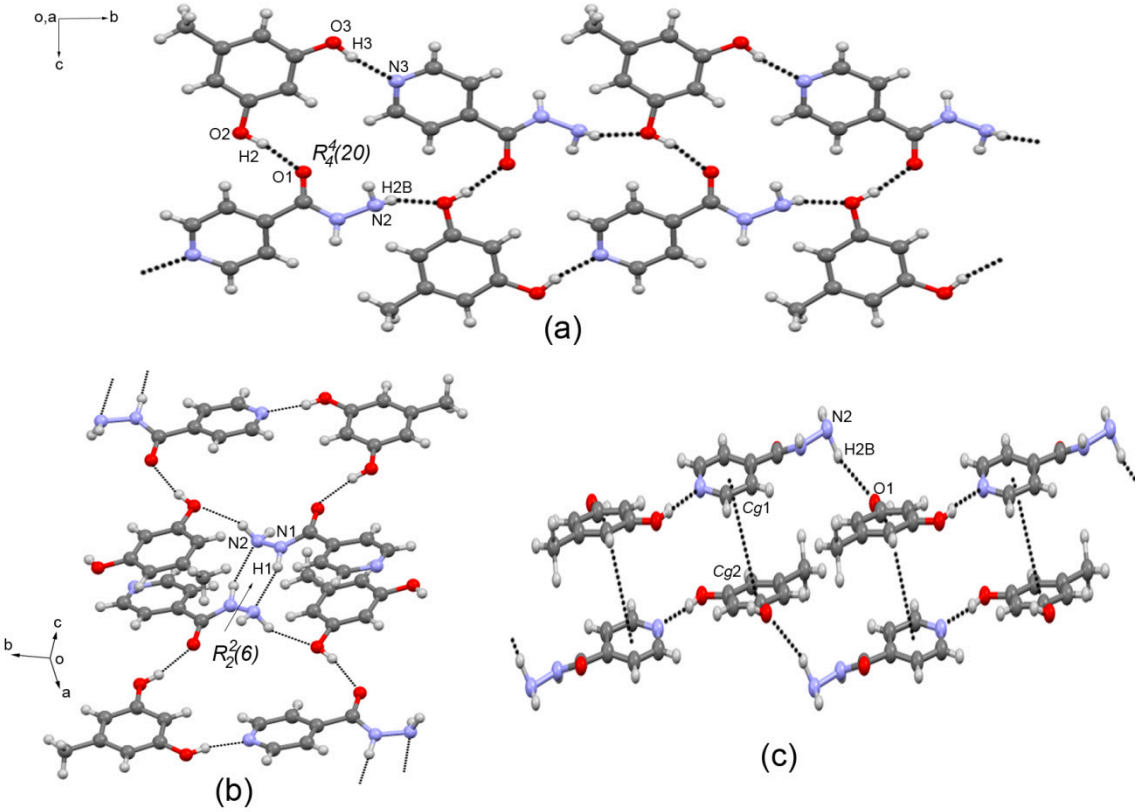

Figure 6. (**a**) 1D supramolecular ribbon of INH-ORC involving the O3–H3···N3, O2–H2···O1, N2–H2B···O2 hydrogen bonds. (**b**) Interlinking of ribbons by the N1–H1···N2 hydrogen bond. (**c**) π-stacking of ORC and INH molecules. Dashed lines represent hydrogen bonds.

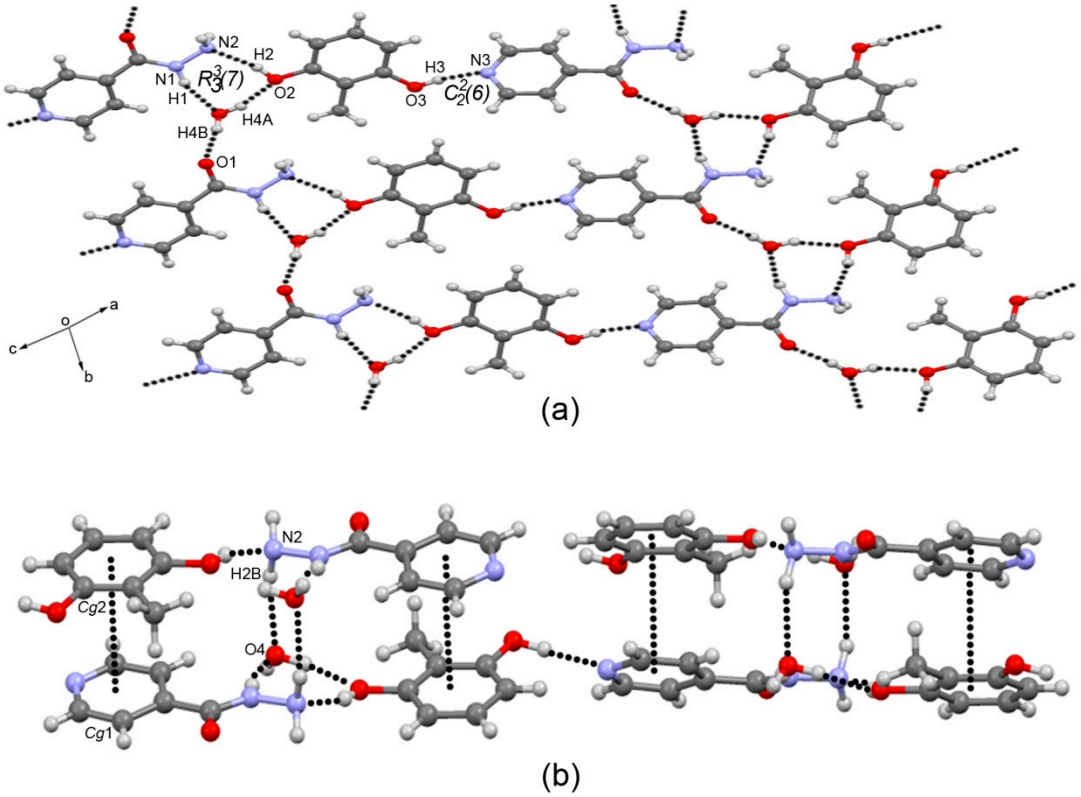

Figure 7. (**a**) Supramolecular sheet of INH-MER–H_2O involving the O3–H3···N3, O2–H2···N2, O4–H4A···O2, O4–H4B···O1, and N1–H1···O4 hydrogen bonds. (**b**) Interlinking of ribbons by the N1–H1···N2 hydrogen bond and π-stacking of MER and INH molecules. Dashed lines represent hydrogen bonds.

INH-PLG cocrystal. The crystal structure of the mechanochemically obtained INH-PLG cocrystal is similar to the one reported in [37]. The isoniazid-phloroglucinol cocrystal crystallizes in the monoclinic $P2_1/c$ space group with two different molecules of INH and one molecule of PLG (in the C_{3h} conformation) in the asymmetric unit. Two of the hydroxyl groups form O–H···N (synthon I) hydrogen bonds (O4–H4···N6 and O3–H3···N3), and the other forms the O5–H5···N5 (synthon V) hydrogen bond. The angles between the pyridine ring and the hydroxyl group plane are 126.23° and −133.80° (C4–N3–H3A–O3 and C11–N6–H4B–O4 torsion angles). A central supramolecular tape is formed by a set of N-H···O (synthon VII) (N4-H4···O1; N5-H5B···O2), N–H···N (synthon VIII) (N1–H1···N2), O–H···N (O5–H5···N5) (synthon V), and N–H···O (synthon III) (N2–H2B···O5) hydrogen bonds showing adjacent $R^2_2(6)$, $R^3_3(10)$, $R^2_2(10)$ motifs extended along the (2 4 −5) plane (Figure 9). A supramolecular sheet is formed when INH and PLG molecules are linked to the central tape by the O4–H4···N6, O3-H3···N3 (synthon I) hydrogen bonds in an almost perpendicular way with C4–N3–H3A–O3 = 126.23° and C11–N6–H4B–O4 = 133.80° torsion angles, similar to that observed in the phloroglucinol-isonicotinamide hydrate cocrystal and the resorcinol-4-pyridine-carboxaldehyde cocrystal [38,39]. The interconnection of supramolecular sheets is given by the N2-H2A···O2 (synthon III), O3–H3···N3, and O4–H4···N6 (synthon I) hydrogen bonds, generating the 3D supramolecular array.

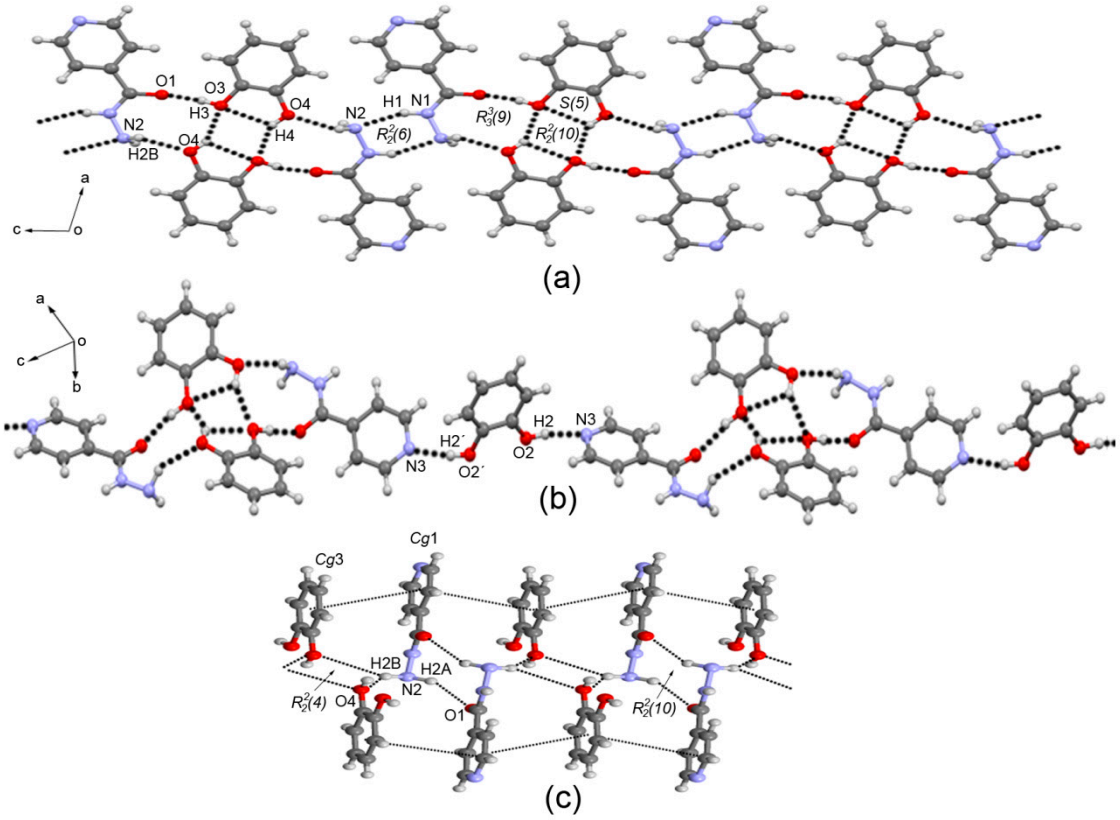

Figure 8. (**a**) Supramolecular tape of INH-CAT involving the O4-H4···O3, N2–H2B···O4, O3–H3···O1, and N1–H1···N2 hydrogen bonds. (**b**) Interlinking of supramolecular tapes by the O2–H2···N3 hydrogen bond. (**c**) π-stacking of CAT and INH molecules. Dashed lines represent hydrogen bonds.

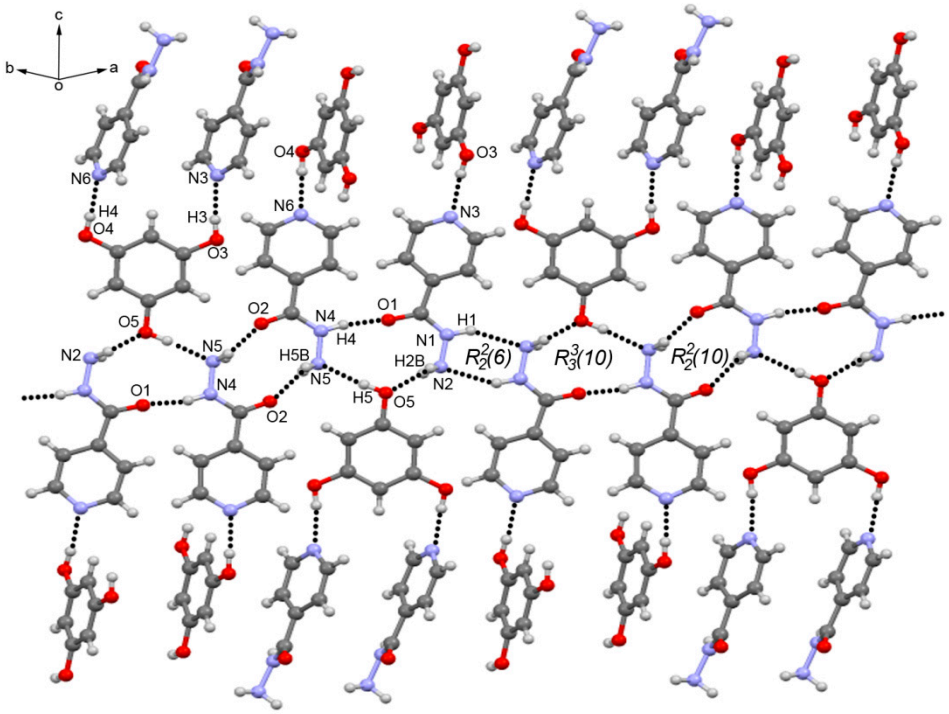

Figure 9. Supramolecular sheet of INH-PLG involving N–H···O, N–H···N, N–H···O, and O–H···N hydrogen bonds. Dashed lines represent hydrogen bonds.

INH-PYR cocrystal. The isoniazid-pyrogallol cocrystal crystallizes in the triclinic *P*-1 group with one molecule of INH and one molecule of PYR in the *anti* conformation in the asymmetric unit (PYR form the O2–H2···O4 *S(5)* intramolecular hydrogen bond). PYR dimerization (synthon IX) occurs via O2–H2···O4 hydrogen bonds $R^2_2(10)$ motif in a similar way to the INH-CAT cocrystal. The PYR dimer is linked to two INH molecules by the N1–H1···O2 (synthon IV) and O4–H4A···N2 (synthon V) hydrogen bonds, depicting a $R^3_3(7)$ motif, forming an INH_2-PYR_2 centrosymmetric tetramer and showing a set of $R^3_3(7)$, $R^2_2(10)$, *S(5)* hydrogen bond motifs. A bidimensional supramolecular sheet, extended along the (1 1 1) plane, is formed by the propagation of the INH_2–PYR_2 by the O3–H3···N3 (synthon I) and N2–H2B···O1 (synthon VI) hydrogen bonds, forming $C^2_2(14)$ chains (Figure 10a). The 1,2,3-trisubstituted PYR allowed for the formation of a finite dimer assembly like CAT, as well as the formation of an infinite chain as in ORC and MER. The angle between the pyridine ring and the hydroxyl group plane is −98.55° (C4-N3-H3A-O3). The third dimensional supramolecular array is given by the interlinking of sheets by the N2-H2A···O3 (synthon III) hydrogen bond depicting a $C^2_2(8)$ motif (Figure 10b).

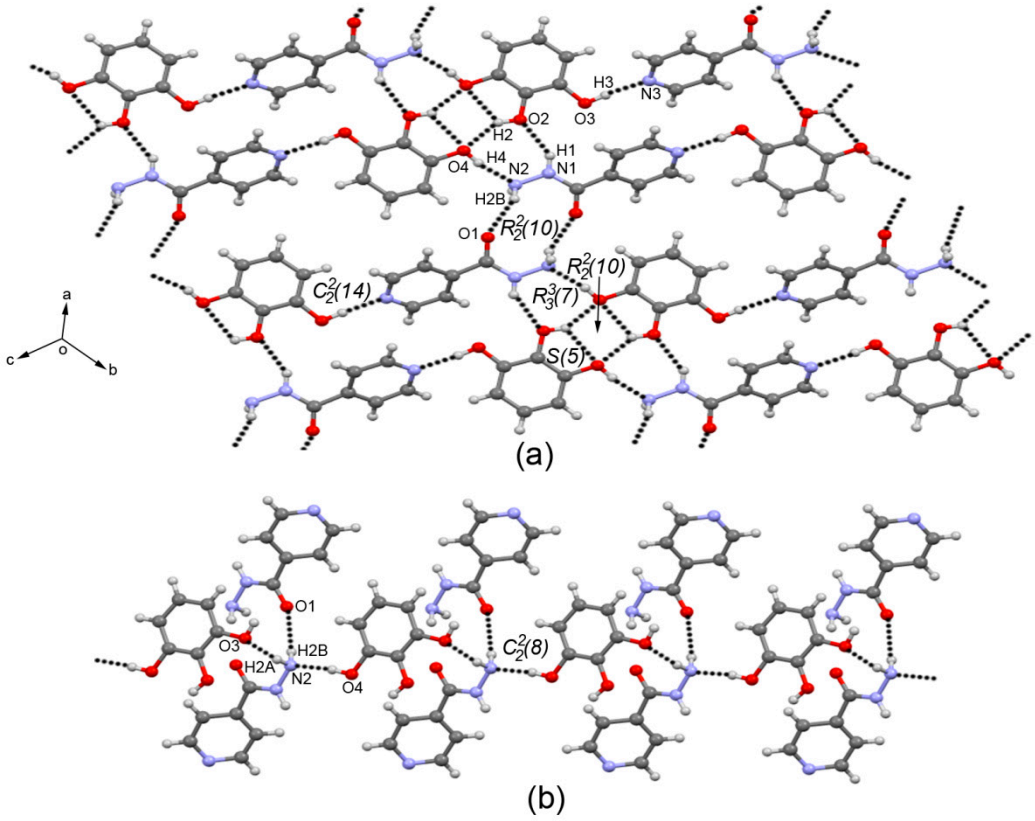

Figure 10. (**a**) Supramolecular sheet of INH-PYR involving the N1–H1···O2, O4–H4A···N2, O3–H3···N3, and N2–H2B···O1 hydrogen bonds. (**b**) Interlinking of sheets by the N2–H2A···O3 hydrogen bonds. Dashed lines represent hydrogen bonds.

An analysis of the supramolecular synthons found in the cocrystals (Figure 5) revealed that the phenol-pyridine heterosynthon (synthon I) is present in the five cocrystals, indicating the hierarchy of this synthon [38,40,41] over the other possibilities. The (terminal) N–H–phenol (synthon III) is the second dominant found in the cocrystals, except in the INH-MER–H_2O cocrystal, which due to the presence of water in the crystalline structure led to the formation of the phenol-hydrazide (synthon V) heterosynthon. The presence of crystallographic independent molecules of INH or the polyphenol, as well as the *ortho*-hydroxy and trihydroxy substitution, caused the formation of six different synthons in the INH-CAT, INH-PLG, and INH-PYR cocrystals.

Polyphenol conformation affects the supramolecular arrangement. In the bis-phenols (ORC, MER, and CAT) when the hydroxyl groups adopt an *anti* conformation, a linear chain is formed as in INH-MER-H_2O cocrystal. On the other hand, a *syn* conformation leads to the formation of a finite motif as in the INH-ORC cocrystal or dimerization as CAT. In the case of the INH-PLG cocrystal, two of the hydroxyl groups point in the same direction (C_{3h} conformation), forming a finite motif. In the INH-PYR cocrystal two hydroxyl groups point in the same direction, generating the dimerization of PYR; meanwhile, the third hydroxyl group points to the opposite direction, leading to the formation of a linear chain.

4. Conclusions

Cocrystals of isoniazid with polyphenolic coformers catechol, orcinol, 2-methyl resorcinol, phloroglucinol, and pyrogallol were obtained by the solvent-assisted grinding method. IR spectra and powder X-ray diffraction patterns of the polycrystalline ground powders were different from the starting materials and similar to those obtained for the single crystals. Incorporation of water into the crystalline structure of INH-MER was discovered. The molecular structure of the cocrystals showed the preference for the (phenol) O-H···N (pyridine) and (terminal) N–H···O (phenol) hydrogen bond synthons. The supramolecular architecture of the cocrystals is affected by the conformation and the substitution pattern of the hydroxyl groups in the polyphenols.

Supplementary Materials: The following are available online at http://www.mdpi.com/2073-4352/10/7/569/s1: Figure S1. Infrared (IR) spectra of isoniazid (INH), catechol (CAT), INH-CAT_{powd}, and INH-CAT_{cryst}; Figure S2. IR spectra of INH, orcinol (ORC), INH-ORC_{powd}, and INH-ORC_{cryst}; Figure S3. IR spectra of INH, 2-methylresorcinol (MER), INH-MER_{powd}, and INH-MER–H_2O_{cryst}; Figure S4. IR spectra of INH, phloroglucinol (PLG), INH-PLG_{powd}, and INH-PLG_{cryst}; Figure S5. IR spectra of INH, pyrogallol (PYR), INH-PYR_{powd}, and INH-PYR_{cryst}; Figure S6. Powder X-ray diffraction patterns of INH, CAT, INH-CAT_{powd}, and INH-CAT_{theor}; Figure S7. Powder X-ray diffraction patterns of INH, ORC, INH-ORC_{powd}, and INH-ORC_{theor}; Figure S8. Powder X-ray diffraction patterns of INH, MER, INH-MER_{powd}, and INH-MER-H_2O_{theor}; Figure S9. Powder X-ray diffraction patterns of INH, PLG, INH-PLG_{powd}, and INH-PLG_{theor}; Figure S10. Powder X-ray diffraction patterns of INH, PYR, INH-PYR_{powd}, and INH-PYR_{theor}; Table S1. Characteristic IR frequencies (cm^{-1}) of INH, the polyphenols, the polycrystalline ground powder, and the single crystals.

Author Contributions: Conceptualization, J.S.G.-G.; methodology, A.M.M.M.-S.; formal analysis and investigation, F.J.M.-M., A.P.-C., M.F.-A., M.J.E.-L. and H.G.-O.; writing—original draft preparation, J.S.G.-G.; writing—review and editing, all authors; visualization, J.S.G.-G. All authors have read and agreed to the published version of the manuscript.

Funding: This research was funded by Universidad de la Cañada, grant number PFI-05/17 and FQ-UNAM (PAIP 5000-9112).

Conflicts of Interest: The authors declare no conflicts of interest.

References

1. Kavanagh, O.N.; Croker, D.M.; Walker, G.M.; Zaworotko, M.J. Pharmaceutical cocrystals: From serendipity to design to application. *Drug Discov. Today* **2019**, *24*, 796–804. [CrossRef]
2. Karagianni, A.; Malamatari, M.; Kachrimanis, K. Pharmaceutical Cocrystals: New Solid Phase Modification Approaches for the Formulation of APIs. *Pharmaceutics* **2018**, *10*, 18. [CrossRef] [PubMed]
3. Duggirala, N.K.; Perry, M.L.; Almarsson, Ö.; Zaworotko, M.J. Pharmaceutical cocrystals: Along the path to improved medicines. *Chem. Commun.* **2016**, *52*, 640–655. [CrossRef]
4. Karimi-Jafari, M.; Padrela, L.; Walker, G.M.; Croker, D.M. Creating Cocrystals: A Review of Pharmaceutical Cocrystal Preparation Routes and Applications. *Cryst. Growth Des.* **2018**, *18*, 6370–6387. [CrossRef]
5. Lewinsohn, D.M.; Leonard, M.K.; LoBue, P.A.; Cohn, D.L.; Daley, C.L.; Desmond, E.; Keane, J.; Lewinsohn, D.A.; Loeffler, A.M.; Mazurek, G.H. Official American Thoracic Society/Infectious Diseases Society of America/Centers for Disease Control and Prevention Clinical Practice Guidelines: Diagnosis of Tuberculosis in Adults and Children. *Clin. Infect. Dis.* **2017**, *64*, e1–e33. [CrossRef] [PubMed]

6. Scior, T.; Meneses-Morales, I.; Garcés-Eisele, S.J.; Domeyer, D.; Laufer, S. Antitubercular isoniazid and drug resistance of Mycobacterium tuberculosis—A review. *Arch. Pharm. Pharm. Med. Chem.* **2002**, *335*, 511–525. [CrossRef]
7. Sarcevica, I.; Orola, L.; Veidis, M.V.; Podjava, A.; Belyakov, S. Crystal and Molecular Structure and Stability of Isoniazid Cocrystals with Selected Carboxylic Acids. *Cryst. Growth Des.* **2013**, *13*, 1082–1090. [CrossRef]
8. Swapna, B.; Maddileti, D.; Nangia, A. Cocrystals of the Tuberculosis Drug Isoniazid: Polymorphism, Isostructurality and Stability. *Cryst. Growth Des.* **2014**, *14*, 5991–6005. [CrossRef]
9. Aitipamula, S.; Wong, A.B.H.; Chow, P.S.; Tan, R.B.H. Novel solid forms of the anti-tuberculosis drug, Isoniazid: Ternary and polymorphic cocrystals. *CrystEngComm* **2013**, *15*, 5877–5887. [CrossRef]
10. Mashhadi, S.M.A.; Yunus, U.; Bhatti, M.H.; Tahir, M.N. Isoniazid cocrystals with anti-oxidant hydroxy benzoic acids. *J. Mol. Struct.* **2014**, *1076*, 446–452. [CrossRef]
11. Kocaçalışkan, I.; Talan, I.; Terzi, I. Antimicrobial activity of catechol and pyrogallol as allelochemicals. *Z. Naturforsch. C* **2006**, *61*, 639–642. [CrossRef] [PubMed]
12. Tyagi, B.; Dubey, A.; Verma, A.; Tiwari, S. Antibacterial activity of phenolics compounds against pathogenic bacteria. *Int. J. Pharm. Sci. Rev. Res.* **2015**, *35*, 16–18.
13. Sarma, B.; Saikia, B. Hydrogen bond synthon competition in the stabilization of theophylline cocrystals. *CrystEngComm* **2014**, *16*, 4753–4765. [CrossRef]
14. Magaña-Vergara, N.E.; de la Cruz-Cruz, P.; Peraza-Campos, A.L.; Martínez-Martínez, F.J.; González-González, J.S. Mechanochemical Synthesis and Crystal Structure of the Lidocaine-Phloroglucinol Hydrate 1:1:1 Complex. *Crystals* **2018**, *8*, 130. [CrossRef]
15. Bolla, G.; Sanphui, P.; Nangia, A. Solubility Advantage of Tenoxicam Phenolic Cocrystals Compared to Salts. *Cryst. Growth Des.* **2013**, *13*, 1988–2003. [CrossRef]
16. Sanphui, P.; Goud, N.R.; Khandavilli, U.B.R.; Nangia, A. Fast Dissolving Curcumin Cocrystals. *Cryst. Growth Des.* **2011**, *11*, 4135–4145. [CrossRef]
17. Karki, S.; Friscic, T.; Fabian, L.; Jones, W. New solid forms of artemisinin obtained through cocrystallisation. *CrystEngComm* **2010**, *12*, 4038–4041. [CrossRef]
18. *CrysAlisPro*, version 1.171.36.32; Oxford Diffraction Ltd.: Abingdon, UK, 2013.
19. Clark, R.C.; Reid, J.S. The analytical calculation of absorption in multifaceted crystals. *Acta Crystallogr.* **1995**, *A51*, 887–897. [CrossRef]
20. Sheldrick, G.M. SHELXT—Integrated space-group and crystal-structure determination. *Acta Crystallogr.* **2015**, *A71*, 3–8. [CrossRef]
21. Sheldrick, G.M. Crystal structure refinement with SHELXL. *Acta Crystallogr.* **2015**, *C71*, 3–8.
22. Farrugia, L.J. WinGX and ORTEP for Windows: An update. *J. Appl. Crystallogr.* **2012**, *45*, 849–854. [CrossRef]
23. Macrae, C.F.; Edgington, P.R.; McCabe, P.; Pidcock, E.; Shields, G.P.; Taylor, R.; Towler, M.; van de Streek, J. Mercury: Visualization and analysis of crystal structures. *J. Appl. Crystallogr.* **2006**, *39*, 453–457. [CrossRef]
24. Gunasekaran, S.; Sailatha, E.; Seshadri, S.; Kumaresan, S. FTIR, FT Raman spectra and molecular structural confirmation of isoniazid. *Indian J. Pure Appl. Phys.* **2009**, *47*, 12–18.
25. Saucedo-Balderas, M.M.; Delgado-Alfaro, R.A.; Martínez-Martínez, F.J.; Ortegón-Reyna, D.; Bernabé-Pineda, M.; Zúñiga-Lemus, O.; González-González, J.S. Synthesis, Molecular Structure of Diethyl Phenylenebis(Methylene)Dicarbamates and FTIR Spectroscopy Molecular Recognition Study with Benzenediols. *J. Braz. Chem. Soc.* **2015**, *26*, 396–402. [CrossRef]
26. Mohammed-Zieglera, I.; Billes, F. Vibrational spectroscopic calculations on pyrogallol and gallic acid. *J. Mol. Struct. THEOCHEM* **2002**, *618*, 259–265. [CrossRef]
27. Steiner, T. The Hydrogen Bond in the Solid State. *Angew. Chem. Int. Ed.* **2002**, *41*, 48–76. [CrossRef]
28. Hunter, C.A.; Sanders, J.K.M. The nature of π–π interactions. *J. Am. Chem. Soc.* **1990**, *112*, 5525–5534. [CrossRef]
29. Bernstein, J.; Davis, R.E.; Shimoni, L.; Chang, N.L. Patterns in Hydrogen Bonding: Functionality and Graph Set Analysis in Crystals. *Angew. Chem. Intl. Ed. Engl.* **1995**, *34*, 1555–1573. [CrossRef]
30. Vedernikova, I.; Proynov, E.; Salahub, D.; Haemers, A. Local atomic and orbital reactivity indices from density functional calculations for hydrogen-bonded 1,2-dihydroxybenzene. *Int. J. Quantum Chem.* **2000**, *77*, 161–173. [CrossRef]

31. Khan, M.; Enkelmann, V.; Brunklaus, G. Solid-State NMR and X-ray Analysis of Structural Transformations in O−H···N Heterosynthons Formed by Hydrogen-Bond-Mediated Molecular Recognition. *J. Org. Chem.* **2009**, *74*, 2261–2270. [CrossRef]
32. Veidis, M.V.; Orola, L.; Mutikainen, I.; Sarcevica, I. The conformation of pyrogallol as a result of cocrystallization with N-heterocyclic bases. *CrystEngComm* **2012**, *14*, 7253–7257. [CrossRef]
33. Braun, D.E.; Tocher, D.A.; Price, S.L.; Griesser, U.J. The complexity of hydration of phloroglucinol: A comprehensive structural and thermodynamic characterization. *J. Phys. Chem. B* **2012**, *116*, 3961–3972. [CrossRef] [PubMed]
34. Mukherjee, A.; Grobelny, P.; Thakur, T.S.; Desiraju, G.R. Polymorphs, Pseudopolymorphs, and Co-Crystals of Orcinol: Exploring the Structural Landscape with High Throughput Crystallography. *Cryst. Growth Des.* **2011**, *11*, 2637–2653. [CrossRef]
35. Thakuria, R.; Cherukuvada, S.; Nangia, A. Crystal Structures of Pyrogallol, Its Hydrate, and Stable Multiple *Z*′ Cocrystals with N-Heterocycles Containing Metastable Conformers of Pyrogallol. *Cryst. Growth Des.* **2012**, *12*, 3944–3953. [CrossRef]
36. Gangavaram, S.; Raghavender, S.; Sanphui, P.; Pal, S.; Manjunatha, S.G.; Nambiar, S.; Nangia, A. Polymorphs and Cocrystals of Nalidixic Acid. *Cryst. Growth Des.* **2012**, *12*, 4963–4971. [CrossRef]
37. Kamalakaran, A.S. Molecular Adducts of Isoniazid: Crystal Structure, Electronic Properties, and Hirshfeld Surface Analysis. *J. Struct. Chem.* **2018**, *59*, 1518–1533. [CrossRef]
38. Vishweshwar, P.; Nangia, A.; Lynch, V.M. Supramolecular synthons in phenol–isonicotinamide adducts. *CrystEngComm* **2003**, *5*, 164–168. [CrossRef]
39. Khan, M.; Enkelmann, V.; Brunklaus, G. O-H···N Heterosynthon: A Robust Supramolecular Unit for Crystal Engineering. *Cryst. Growth Des.* **2009**, *9*, 2354–2362. [CrossRef]
40. Corpinot, M.K.; Kresimir Bucar, D.K. A Practical Guide to the Design of Molecular Crystals. *Cryst. Growth Des.* **2019**, *19*, 1426–1453. [CrossRef]
41. Bis, J.A.; Vishweshwar, P.; Weyna, D.; Zaworotko, M.J. Hierarchy of Supramolecular Synthons: Persistent Hydroxyl···Pyridine Hydrogen Bonds in Cocrystals That Contain a Cyano Acceptor. *Mol. Pharm.* **2007**, *4*, 401–416. [CrossRef]